On site mirror tests for Cherenkov telescopes

J. Dipold[a,*], M. C. Medina[c], B. García[b], V. de Souza[a], E. Rasztocky[c], A. Mancilla[1], J. Maya[1], J. J. Larrarte[c]

[a]*Instituto de Física de São Carlos, Universidade de São Paulo, São Carlos, SP, Brazil.*
[b]*Universidad Tecnológica Nacional, FR-Mendoza, Argentina.*
[c]*Instituto Argentino de Radioastronomía, CCT La Plata-CONICET, Argentina.*

Abstract

Imaging Atmospheric Cherenkov Technique (IACT) has provided very important discoveries in Very High Energy (VHE) γ-rays astronomy for the last two decades, being exploited mainly by experiments as H.E.S.S. [1], VERITAS[2] and MAGIC[3]. The same technique will be used by the next generation of γ-ray telescopes, CTA (Cherenkov Telescope Array), which is conceived to be an Observatory composed by two arrays strategically placed in both hemispheres, Northern and Southern. Each site will consist of several tens of Cherenkov telescopes of different sizes and will be equipped with about 5000 m^2 of reflective surface. Because of its large size, the reflector of a Cherenkov telescope is composed of many individual mirror facets. Cherenkov telescopes operate without any protective system from weather conditions demanding mirrors to resist several environmental aggressions. In order to fulfill the specifications on optical properties, mechanical behavior and costs, different technological solutions are under study. Most of them involve composite structures which behavior against ambient aggression has not been exhaustively studied until now.This paper describes the experiments carried out to test the robustness of optical and mechanical properties of prototype mirror facets for CTA under real observation conditions. A dedicated facility was built at one of the Argentinean candidate sites to host the CTA Southern array. We monitored the mechanical and optical performance of the mirrors along one year and we study the behavior of the mirrors in presence of water vapor condensation. The study presented here shows im-

*Instituto de Física de São Carlos, Universidade de São Paulo, São Carlos, SP, Brazil. E-mail address: jessica.dipold@gmail.com (J. Dipold)

Preprint submitted to Nuclear Physics B *August 25, 2015*

portant guidelines in the selection procedure of mirror technologies used in future Cherenkov telescopes.

Keywords: Cherenkov Telescopes, mirrors characterization, CTA

1. Introduction

The Cherenkov Telescope Array (CTA) will dramatically improve the current instruments' sensitivity in a factor of ten for a broad energy range (from 50 GeV to 100 TeV), also achieving an angular resolution five times better than typical values of around $0.1°$. It will consist of over 100 telescopes operating in two different sites, in the Northern and Southern hemispheres. CTA is designed to allow the study of the origin of cosmic rays through the investigation of acceleration processes, black hole particle accelerators and the examination of nature beyond the Standard Model, searching for dark matter and effects of quantum gravity [4].

The mirror facets is a crucial part of Cherenkov telescopes, therefore, it is necessary to test different manufacture techniques to find which one has the best cost/effectiveness ratio while keeping the desired quality requirements. Among several characteristics which determine the quality of a reflective surface, two main ones should be considered first in the qualification of a mirror facet: the Point Spread Function (PSF) and the reflectivity. The PSF of a facet is determined by its mechanical and optical properties. The size of the PSF should be typically smaller than the photomultiplier pixel. The reflectivity is given by the coating material and fabrication technique and it should be maximized between 300 and 450 nm. Current experiments [5, 6] use mirrors with aluminium as a reflective material and protective layers (e.g. quartz) to ensure resistance against weather conditions. These mirrors usually lose 3-4% of its reflectance per year [7], which requires re-coating every 5 years.

This work aims to assist in the choice of both the mirror facets and the site where the Observatory will be constructed. In order to do that, we developed a facility in San Antonio de los Cobres (SAC), one of the proposed sites for CTA. The facility was constructed to study the behavior of prototype mirrors in the operational conditions of the site. The mirror facets proposed to equip CTA telescopes are large and heavy. The midium size telescope (MST) is going to have hexagonal mirror facets with 1.2 m face-to-face and weight around 25 kg. The dimensions of the facets and the remoteness of the candidate sites make it difficult to transport them to a well equipped laboratory in order to measure its properties. To avoid these difficulties and still obtain relevant data, we developed this facility in SAC to measure the main properties of the mirrors as a function of the exposition time.

We exposed two prototype mirrors from November/2013 until June/2014. One mirror was coated with aluminium and a quartz protective layer, the other one is a dielectric mirror. During this period, two PSF and reflectivity measurement campaigns were done, with the aim to analyze if the shape of the mirrors changed and if their reflectivity was damaged. We also studied the formation of condensation on its surfaces. We calculated the time the mirrors were condensed during the night, giving an estimation of the operational time lost due to condensation if a Cherenkov telescope would operate in the SAC site.

In section 2, we describe the experimental setup and the data taking procedure. In section 3, we analyze the data and in section 4 we conclude the study.

2. Experimental setup and data taking

2.1. Site description

The San Antonio de los Cobres site is located at Lat. 24° 02' 42.7" S and Lon. 66° 14' 05.8" W, in the Province of Salta, Argentina. Altitude of the site is 3600 meters a. s. l. It is a flat area of approximately 4 km $\times$ 5 km surrounded by hills of hundreds of meters high above the plateau (see Fig. 1). In the region, a semi-arid continental climate dominates, with high temperature fluctuations between day and night. Since 2010, several instruments have been installed to monitor the general atmospheric conditions (temperature, humidity, wind speed, etc.), the night sky background and the cloud coverage (see [8] and [9] for details).

2.2. Installation

Inside the fenced area at the SAC site, the two MST mirrors were installed in a suitable position for the tests. The system consists of independent structures to hold each mirror in three different positions: *parking* (mirrors facing down), *observation* (mirrors facing up, at -45° from the zenith) and *test* (mirrors in vertical position facing the horizon). During daytime the mirrors remain at *parking* position. After sunset, they move to *observation*, coming back to *parking* at sunrise. The mechanical structure was calculated in order to support by far the standard facets weight ($\sim$ 30 kg) and to stay still under extreme wind blow.

Each mirror is viewed by an IP camera (Ubiquiti AirCam [1]) and images of the mirrors are taken every 10 minutes. In order to distinguish the fog or ice formation on the mirror surfaces when it happens, they are tangentially illuminated by high intensity white LED (SMD cold white 5060 [2]) during night (see Fig. 2) in order to increase scattering effects when water particles laid over the reflective surfaces. Temperature (DS18B20) and humidity (IH-4000) sensors are installed at the mirrors surface in order to permanently monitor their behavior.

The complete system is controlled and managed by an SBC (Single Board Computer) TS-7260, which has a built-in Embedded Linux operating system, allowing the control of various associated devices using the RS232 ports available (weather station, sensors and motor controller), control the IP cameras and a self-made communication system. With this system the meteorological data and camera images are acquired to be stored on a flash drive, the reflectors are switched on and the mirrors positioned automatically. A link that works through a high power outdoor wireless access point (model TL-WA5210G AP) with a grilled 24dBi antenna allows to transfer information to servers located in Mendoza, serving also for remote diagnostics and monitoring. After collecting the data (images and sensors data), the SBC is autonomously synchronized once per day to Mendoza servers. The data was available by a secured ftp server for the project members.

Because the entire system should operate in an area lacking of an electricity grid, a photo-voltaic system powering the controller, the reflectors, the cameras, the engines and the communication system was installed. A scheme with the different components of the control system is showed in figure 3.

2.3. Optical measurement setup

A 2f system [10] was mounted in order to measure the PSF and focal length of the mirrors. The blueprint of the equipment is shown in figure 4. Its parts were a variable height tripod, a high-power blue LED collimated by simple lenses to work as a punctual source, a white screen to observe the image formed by the mirrors, a laser distance measurer to learn the

[1] http:www.ubnt.com

[2] http://dled.com.ar/leds-5060-exterior

distance of the system from the mirror and a commercial digital camera. The distance between the mirror and the screen was changed in steps of 50 cm around the quoted 2f distance. A picture of the screen was taken and the size of the PSF was calculated as the radius containing 80% of the image light. Figure 5 shows an example of the pictures taken. We can determine the minimum PSF size and the 2f distance in a single experiment through an analysis of the size variation of the PSF with the distance between the light source and the image.

The reflectivity of the mirror surfaces was measured with a commercial Ocean Optics® spectrometer of the Jaz® model. Jaz® is a portable spectrometer with a pulsed Xenon lamp, which emits light that is sent through an optical fiber to the mirror surface. The light is then reflected back to the spectrometer through a second optical fiber. Both fibers are protected by a metal tube. Since our measurements were made at daylight under the sun, a black head was adapted on the top of the tube where the optical fibers are located to isolate the analyzed surface from the background light. The spectrometer is built such that it can analyse wavelength-depended light intensities between 250 and 850 nm.

Before each reflectivity measurement a dark and a reference spectrum were taken. The former is done by putting the reference mirror over the black head with the Xenon lamp turned off, and the latter with the lamp turned on. Due to the reduced width (radius) of the optical fibers, the spectrometer measure only the local reflectivity, which is defined as the ration between the measured spectrum and the reference one. In order to obtain an estimate of the global reflectivity of the mirror surface we repeated the measurements in twelve different points around the aluminium coated hexagonal mirror and in ten points around the dielectric circular one, as shown in figure 6. We quote an overall reflectivity of the mirror facet as the average of these measurements.

During the period from November/2013 to June/2014, two different mirrors were exposed at the SAC - Mirror Test System (MTS). One of the mirrors was build at INAF Brera [11] using the cold slump technique. The glass substratum is molded to the desired shape and coated with aluminium. We have also used a dielectric mirror taken from H.E.S.S. I telescopes [12]. Out of 1600 mirror facets currently in use in H.E.S.S. I telescopes, 100 mirrors were done with a dielectric coating. Details of the construction of these mirrors can be found in the references given above. We refer to the mirrors as *aluminium* and *dielectric* throughout this paper.

The mirror facets exposed in the SAC-MTS were concave and had quoted focal positions around 16 meters for the aluminium and 15 meters for the dielectric. The reflectivity, PSF size and 2f distance were measured with six months of interval, characterizing the deterioration of the mirror after exposition to the environmental conditions.

During the night, a picture was automatically taken of each mirror every 10 minutes. Figure 7 shows an example of the pictures taken by the automatic web-cams. The left figure shows a clean mirror and the right one a mirror fully condensed. These pictures were analyzed to extract the amount of time and area of condensation of the mirrors under the site weather conditions. Table 1 shows a summary of mirrors used in the experiments.

3. Data analysis

3.1. Variation of the 2f distance and of the PSF size

Figure 8 illustrates the analysis done to determine the PSF size as the radius containing 80% of the light in the image formed by the mirror when illuminated by a point source. Figure 9(a) corresponds to the spot size of the aluminun mirror in November at 33 m. Figure 9(b) corresponds to the spot size of the dieletric mirror in November at 31.5 m. Figure 9 shows the PSF size as a function of the distance between the mirror and the screen on which the image was formed. The minimum PSF was calculated by fitting the data with two straight lines with a break point. The break point was allowed to vary in the fitting procedure. The distance of the minimum is the 2f distance. Table 2 summarizes the calculated 2f and the corresponding PSF size.

It is clear from this analysis that the 2f distance and the PSF size did not change in both mirrors significantly in one month. The 2f distance changed by 0.2 m in both cases. The PSF size changed only 0.1 cm in one case. However, the measured size of the PSF far from the 2f distance changed significantly for both mirrors as seen in figure 9. This changes were caused by different experimental conditions and therefore are an instrumental artefact instead of a change in the mirror shape. The illumination and background light were not the same in both measurements moreover the surface of the mirrors were dirty after one month of of exposition causing an increase of the PSF size.

3.2. Reflectivity measurements

The environmental conditions, such as wind, rain and dust, are expected to damage the surface of the mirror, decreasing its reflectivity. The aim of our observations is to verify this effect. We took reflectivity measurements twice, the first time in December 2013 and the second one in June 2014. The relevant range for Cherenkov light observation is between 300 and 450 nm, therefore the analysis of the optical quality of the mirrors was made in this wavelengths interval.

The reflectivity as a function of wavelength for both mirrors is shown in figure 10 for wavelength between 300 and 650 nm. The lines show the mean of all reflectivity values measured along the mirror in the positions shown in figure 6. The hatched zones represent the statistical fluctuation of the mean.

For the aluminium mirror (figure 10(a)), the largest variation is at most 3% in the ranges of 330-340 nm and 400-450 nm. The dielectric mirror (figure 10(b)) shows no significant variation in its reflectivity between the data obtained in December/2013 and June/2014 for the wavelength range between 300 and 450 nm. Two discontinuities in the reflectivity measurements at 520 and 550 nm are shown. In this regions the variation of the reflectivity from December/2013 to June/2014 is larger than in other wavelenghts.

3.3. Condensation calculation

Figure 11 shows a color coded map of the aluminuim mirror in two occasions: when it was not condensed (a) and full of condensation (b). The vertical feature seen in the middle of the image is a support bar which is removed from further analysis.

In extreme conditions as the one shown in figure 11, it is not hard to discriminate mirrors with some condensation, however when small parts of the mirror are condensed the identification must be done by a more sophisticated analysis. The first step of this analysis was to identify the pictures in which the mirror had some condensation. In order to do so, we calculated nine relevant parameters to classify each picture. The parameters were chosen due to its potential to discriminate a mirror with condensation from a mirror without any condensation. Four standard statistical parameters were calculated for the pixel intensity distribution of each picture: average, standard deviation, kurtosis and skewness. Condensed mirror scatters more light and therefore the larger the average intensity is, the surface is more condensed. Condensation usually starts from the borders of the mirror and for a long time only a small part of the surface is condensed. In this cases, there is a big variation of the intensity in the surface, increasing the standard deviation. The kurtosis is smaller for not-condensed mirrors, since they are expected to have intensities close to the average. And the skewness will be larger for condensed mirrors because of their intensity variation on its surface.

Besides the standard statistical parameters, other five proposed by Haralick et al. [13] were used to improve the identification of the mirrors with condensation: second angular momentum, contrast, correlation, entropy and inverse different momentum. Haralick parameters are widely used in image processing [14], pattern recognition [15], edge detection [16] and noise removal [17]. The second angular momentum gives the homogeneity of the picture. Therefore, large second angular momenta are related to not-condensed mirrors. Contrast measures the local variation of intensities, being larger for not-homogeneous pictures. Correlation is a measurement of the linear dependency of the intensity over the image, varying greatly with the observed angle. It is larger for condensed mirrors than for not-condensed ones. Entropy measures the randomness of the intensity distribution of the pictures, being smaller the more homogeneous a picture is. Therefore large entropies are related to condensed mirrors. And the last parameter chosen was the inverse different momentum, considered the inverse of the contrast.

Figure 12 shows the distribution of the nine parameters for a set of 100 images identified by visual inspection as mirrors with (50 images) and without (50 images) condensation. The nine parameters were used as an input for classifier mechanisms. We have used supervised algorithms based on Random Forest [18] techniques implemented in the Weka software [19]. The classification algorithm was trained with the 100 pictures classified by eye as condensed or not. The software combines the nine parameters and removes possible correlation. The output of the analysis is the classification of the picture as containing or not condensation. For more details about the classification techniques see references [18, 19].

Table 3 shows the confusion matrix of the algorithm for both mirrors. The efficiency of the selection is similar for both mirrors. For the aluminium (dieletric) mirror, 92% (97%) of the mirrors known to be condensed were classified as condensed. The set of mirrors known to have no condensation were classified as condensed with 7% (3%) for the aluminium (dieletric) mirror. The mirrors that were badly classified are below 10% of the total. The misclassification percentage is going to be propagated into the final results. The set of mirrors which were selected to have some condensation is considered in the next step of the analysis.

In order to calculate which area of the mirror is condensed and for how long, it is necessary to know which pixels from the selected pictures are condensed. The second step of this analysis is to identify within the condensed mirrors the condensed pixels. Each pixel in the picture corresponds to an area of the mirror.

Figure 13 and 14 shows the pixel intensity as a function of the height in the mirror. Many pictures (100) have been analyzed by visual inspection and we have selected condensed and clean pixels along the height of the mirror. For the aluminium mirror, the first 30 cm were too illuminated, saturating the image. Therefore the first 30 cm at the top of this mirror (large Y values) are not considered in this analysis.

Figure 13 shows how the dependence of the intensity of the reflected light by a clean (blue) and a condensed (yellow) region of the mirror is very different. We fit a second order polynomial function in the lower bound of the two sigma region defining the condensed pixels and used it as a selection curve. The region in orange in figure 13 shows the parameter space in which a pixel is considered to be obscured due to condensation or other effects. Figure 14 shows the equivalent plot for the dielectric mirror.

Other effects may obscure the area of a mirror rather than condensation. The first analysis step selected mirrors with some condensation, however, many pixels in those mirrors are not condensed. Pixels corresponding to dirty or very wet (rain - big water drops) parts of the mirrors also scatter light in abundance. We have tried to identify some of the obscured but not condensed pixels, but we have not reached a high efficiency. Moreover, wet areas of the dielectric mirror reflects light in a very different way from the aluminium mirror. Pixels corresponding to wet areas in the aluminium mirror are often classified as obscured. On the other hand, pixels corresponding to wet areas in the dielectric mirror are often classified as clean. We estimated that the percentage of pixels corresponding to dirty or wet areas in the condensed mirrors sample is not larger than 5%. Therefore, the pixels selected as obscured according to figures 13 and 14 include areas which are not only condensed, but are dirty or wet as well. In this way, the following calculation of the time and area the mirror was obscured represents an upper limit on the condensation time for the aluminium mirror and a lower limit on the condensation time for the dielectric mirror. We use the word obscured from now on to remember the reader the mix between condensed, dirty and wet pixels.

With each pixel classified as obscured, we calculated the time they remained that way. Each picture represents ten minutes of observation time, and for both mirrors the total number of pictures taken is of the order of 6000, providing us with 60000 minutes or 1000 hours of observation. The percentage of time each pixel was obscured is shown in figures 15 and 16, for the aluminium and dielectric mirrors respectively. The top part of the aluminium mirror was removed because the pixels were saturated in that region. As mentioned above, a central column where a support bar was located was also removed from this analysis. We estimate that the misclassification of some mirrors and pixels represents a systematical uncertainty of 4% in the calculation of the obscured time.

The Aluminium mirror 15 condensed mostly in the upper part. The red areas in figure 15 correspond to the maximum condensation time of 18%. The condensation sprays from the top to the bottom of the mirror. A large portion of the mirror is usually condensed.

The dielectric mirror 16 showed a different condensation pattern. The upper and lower part of the mirror condensate more often while the inner part remains most of the time clean.

In figures 17 and 18, we show the relation between the time and area obscured for both mirrors. The Aluminium (figure 17) mirror stays nearly 75% of the time with more than 10% of its surface obscured, and 35% of the time with more than 80% of its surface obscured. The dieletric mirror (figure 18) had only 18 to 26% of its area obscured in the period of observation.

4. Conclusions

Three tests were described in this paper: the measurement of the focal position variation, the reflectivity variation and the condensation time of prototype mirrors exposed to the Santo Antonio de los Cobres site condition.

The PSF and the radius of curvature of both mirrors studied did not change significantly during one month of observation as seen in figure 9. The variation of the size of the PSF far from its minimum is an experimental artfact due to different experimental conditions.

The reflectivity of both mirrors also did not change significantly during 6 months of observation (figure 10). Previous experiments [7] have reported a variation of 3-4% of the reflectivity per year. Considering the same degradation speed one could foresee a variation of 1.5-2% in six months which is much smaller than the dispersion of our measurements as shown in figure 10.

A method to identify condensation in mirror pictures and to classify obscured areas in the mirror was developed. The method uses image analysis and classification algorithms to reach a high selection efficiency. We used the developed technique to study condensation time and area of the prototype mirrors.

We showed different condensation patterns in aluminium and dielectric mirrors in figures 17 and 18. The condensation tend to spray widely over an aluminium mirror and stays concentrated in small portions in the dielectric one. The estimated times of condensation represent a lower limit for the dielectric mirror and an upper limit for the aluminium mirror due to the different misclassification of wet pixels.

The percentage of the condensed area influences the capabilities of the telescopes in several ways. In SAC, dielectric mirrors would have at least 20% of its area obscured for about 2% of the operational time. Aluminium mirrors would have at most 20% of its area obscured for about 6% of the operational time. The relation between obscured time and area is given in figures 17 and 18. The amount of time with large condensation areas of the mirrors would be a serious limitation for a Cherenkov telescope to operate in SAC.

5. Acknowledgments

J. Dipold thanks FAPESP (2012/23676-7) for the scholarship. V. de Souza thanks the Brazilian population for the support via CNPq and FAPESP. The authors thank the support given by the technical team of the Instituto Argentino de Radioastronomia, the government of San Antonio de los Cobres and the Fundacion Capacitar del NOA at the system installation.

6. References

References

[1] F. Aharonian, et al., H.E.S.S. Collaboration, Observations of the Crab nebula with HESS, Astronomy and Astrophysics 457 (2006) 899–915. arXiv:astro-ph/0607333, doi:10.1051/0004-6361:20065351.

[2] VERITAS, Very energetic radiation imaging telescope array system, http://veritas.sao.arizona.edu (2011).

[3] MAGIC, Gamma-ray astronomy at low energies with high sensitivity, `https://magic.mpp.mpg.de` (2015).

[4] M. Actis, G. Agnetta, F. Aharonian, A. Akhperjanian, J. ALEKSIĆ, E. Aliu, D. Allan, I. Allekotte, F. Antico, L. Antonelli, et al., Design concepts for the Cherenkov Telescope Array CTA: an advanced facility for ground-based high-energy gamma-ray astronomy, Experimental Astronomy 32 (2011) 193–316. arXiv:1008.3703, doi:10.1007/s10686-011-9247-0.

[5] M. Doro, D. Bastieri, A. Biland, F. Dazzi, L. Font, M. Garczarczyk, M. Ghigo, E. Giro, F. Goebel, R. Kosyra, E. Lorenz, M. Mariotti, R. Mirzoyan, L. Peruzzo, G. Pareschi, J. Zapatero, Nuclear Instruments and Methods in Physics Research A 595.

[6] K. Bernlohr, et al., The optical system of the H.E.S.S. imaging atmospheric cherenkov telescopes. Part I: layout and components of the system, Astroparticle Physics 20 (2) (2003) 111 – 128. doi:http://dx.doi.org/10.1016/S0927-6505(03)00171-3.

[7] G. Phlhofer, O. Bolz, N. Gtting, A. Heusler, D. Horns, A. Kohnle, H. Lampeitl, M. Panter, M. Tluczykont, F. Aharonian, A. Akhperjanian, M. Beilicke, K. Bernlhr, H. Brst, H. Bojahr, T. Coarasa, J. Contreras, J. Cortina, S. Denninghoff, M. Fonseca, M. Girma, G. Heinzelmann, G. Hermann, W. Hofmann, I. Jung, R. Kankanyan, M. Kestel, A. Konopelko, H. Kornmeyer, D. Kranich, M. Lopez, E. Lorenz, F. Lucarelli, O. Mang, H. Meyer, R. Mirzoyan, A. Moralejo, E. Ona-Wilhelmi, A. Plyasheshnikov, R. de los Reyes, W. Rhode, J. Ripken, G. Rowell, V. Sahakian, M. Samorski, M. Schilling, M. Siems, D. Sobzynska, W. Stamm, V. Vitale, H. Vlk, C. Wiedner, W. Wittek, The technical performance of the HEGRA system of imaging air cherenkov telescopes, Astroparticle Physics 20 (3) (2003) 267 – 291. doi:http://dx.doi.org/10.1016/j.astropartphys.2003.06.001.

[8] I. Allekotte, G. de la Vega, A. Etchegoyen, B. García, A. Mancilla, J. Maya, D. Ravignani, A. Rovero, f. t. CTA Consortium, Sites in Argentina for the Cherenkov Telescope Array Project, ArXiv e-printsarXiv:1307.5014.

[9] R. D. Piacentini, M. Freire, M. I. Micheletti, G. M. Salum, J. Maya, A. Mancilla, B. García, f. t. CTA Consortium, Typical atmospheric aerosol behavior at the Cherenkov Telescope Array candidate sites in Argentina, ArXiv e-printsarXiv:1307.6100.

[10] P. Brun, P.-H. Carton, D. Durand, J.-F. Glicenstein, C. Jeanney, M. C. Medina, P. Micolon, B. Peyaud, Composite mirror facets for ground based gamma ray astronomy, Nuclear Instruments and Methods in Physics Research A 714 (2013) 58–66. arXiv:1301.6988, doi:10.1016/j.nima.2013.01.051.

[11] G. Pareschi, et al., Glass mirrors by cold slumping to cover 100 m2 of the magic ii cherenkov telescope reflecting surface (2008). doi:10.1117/12.790404.

[12] A. Förster, T. Armstrong, P. Chadwick, M. Held, for the CTA Collaboration, Rio de Janeiro, Brasil.

[13] R. M. Haralick, K. Shanmugam, I. Dinstein, Textural features for image classification, IEEE Transactions on Systems, Man, and Cybernetics 3 (1973) 610–621. doi:10.1109/TSMC.1973.4309314.

[14] R. M. Haralick, L. Watson, A facet model for image data, Computer Graphics and Image Processing 15 (2) (1981) 113 – 129. doi:http://dx.doi.org/10.1016/0146-664X(81)90073-3.

[15] R. Haralick, R. Harpaz, Linear manifold clustering in high dimensional spaces by stochastic search, Pattern Recognition 40 (2007) 2672 2684.

[16] R. M. Haralick, Digital step edges from zero crossing of second directional derivatives, IEEE Transactions on Pattern Analysis and Machine Intelligence PAMI 6 (1) (1984) 58–68.

[17] Y. Yasuoka, R. M. Haralick, Peak noise removal by a facet model, Pattern Recognition 16 (1) (1983) 23 – 29. doi:http://dx.doi.org/10.1016/0031-3203(83)90004-3.

[18] L. Breiman, Random forests, Machine Learning 45 (1) (2001) 5–32.

[19] M. Hall, E. Frank, G. Holmes, B. Pfahringer, P. Reutemann, I. H. Witten, The WEKA data mining software: an update, SIGKDD Explorations Newsletter 11 (1) (2009) 10–18.

Origin	**Type**	**Size (m)**	**Number of exposed days**
INAF-Brera	Glass/Aluminium	1.2 (face-to-face)	103
H.E.S.S.	Glass/Dielectric	0.30 (radius)	103

Table 1: Summary of the mirrors used in the experiment.

	November/2013		**December/2013**	
	2f (m)	PSF (cm)	2f (m)	PSF (cm)
Aluminium	33.0	1.4	32.8	1.3
Dielectric	30.8	1.5	30.6	1.5

Table 2: Point Spread Function (PSF) size and 2f distance calculated for the two mirrors in the two months in which the measurement was done.

(a)

Classification:	Condensed	Not-Condensed	True:
	92%	8%	Condensed
	7%	93%	Not-Condensed

(b)

Classification:	Condensed	Not-Condensed	True:
	90%	10%	Condensed
	3%	97%	Not-Condensed

Table 3: Confusion matrix of classification algorithm for (a) aluminium and (b) dielectric mirrors.

Figure 1: Panoramic view of the San Antonio de los Cobres site.

Figure 2: Experimental setup installed in SAC. The picture shows the mirror held by its adjustable support, the LED stripe which illuminated the mirrors while the picture is taken by the web-cam every 10 minutes.

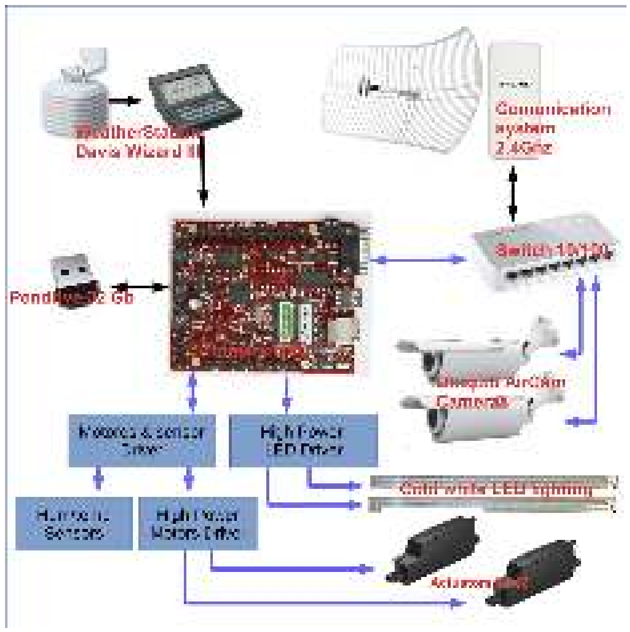

Figure 3: Comm diagram.

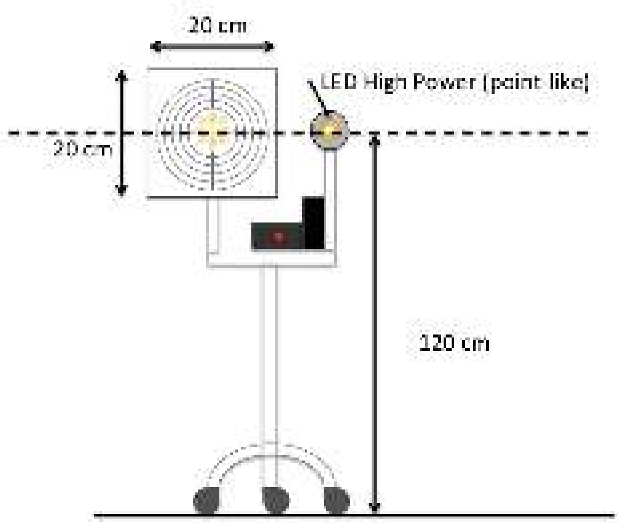

Figure 4: Blueprint of the 2f system used to take a picture of the image done by the mirror under the illumination of a point source. The LED source and the screen target over which the image was formed and the laser distance measurer are shown. The camera which was used to take the picture is not showed.

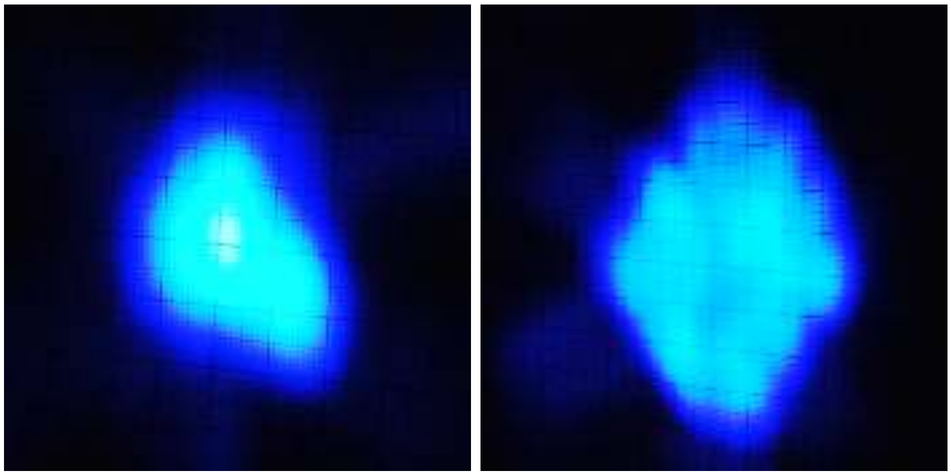

Figure 5: Pictures taken from the image formed over the screen of the 2f system. The left picture is the image formed by the aluminium coated mirror close to its 2f distance. The right picture is the image formed by the dielectric mirror close to its 2f distance. The checked scale was used to determine the size of the PSF in centimeters.

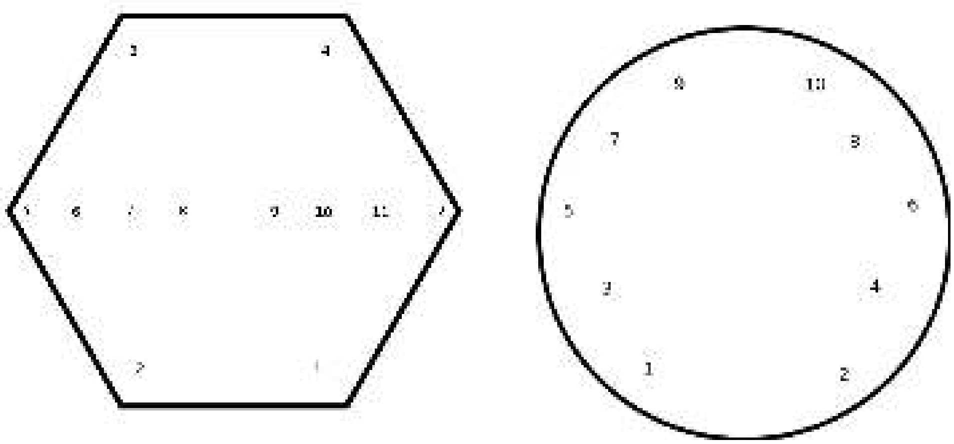

(a) (b)

Figure 6: Approximate positions of the reflectivity measurements for the (a) aluminum hexagonal and (b) dielectric circular mirrors. The measurements could not be taken in the center of the mirrors because of the positioning of the sensors in their surfaces. Figures not in scale.

Figure 7: Example of pictures taken by the web-cam. The left image shows the mirror without condensation. The right image shows the mirror completely covered by condensation.

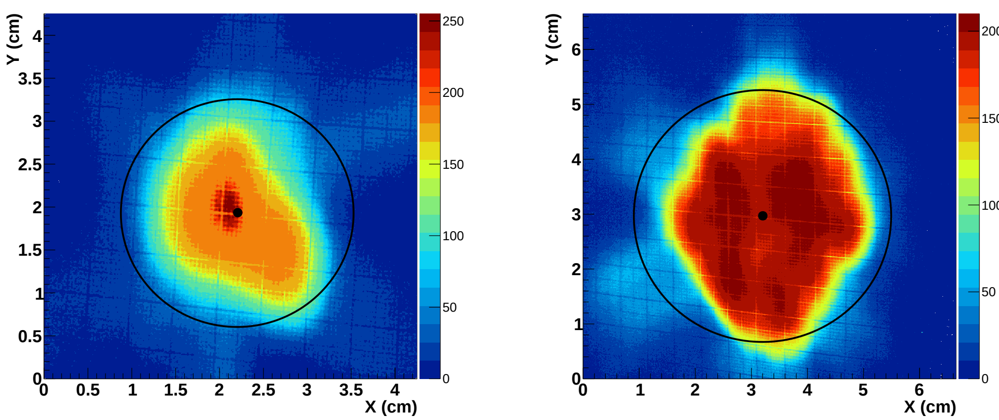

(a) (b)

Figure 8: Point Spread Function (PSF) determination for the (a) aluminium (at 33 m) and (b) dielectric (at 31.5 m) mirrors. The central black dots show the barycenter of the image from which the radius is measured. The black circle shows the radius containing 80% of the light which is the PSF size. The color code shows the light intensity ranging from 0 to 256.

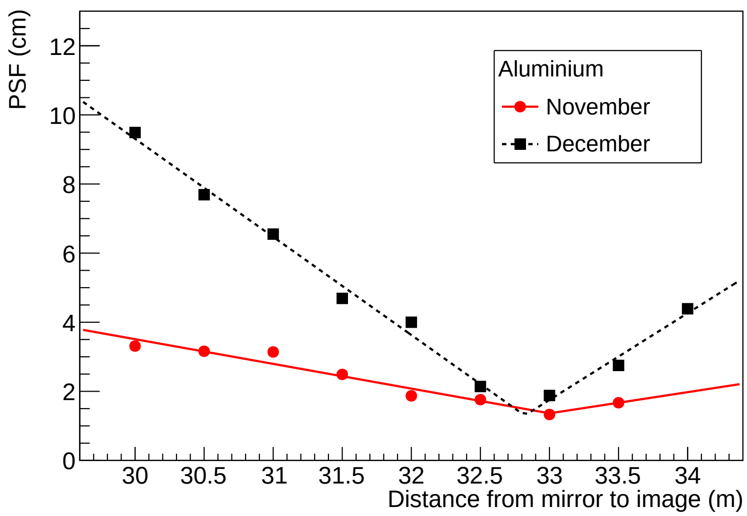

(a)

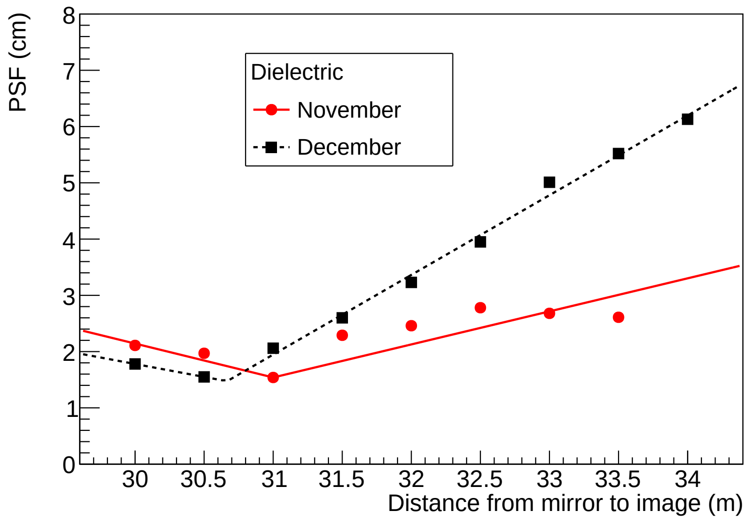

(b)

Figure 9: Point Spread Function (PSF) as a function of the distance from the mirror to the image for the (a) aluminium and (b) dielectric mirrors. The full and dashed lines represent fits of the points. See text for the details about the fit.

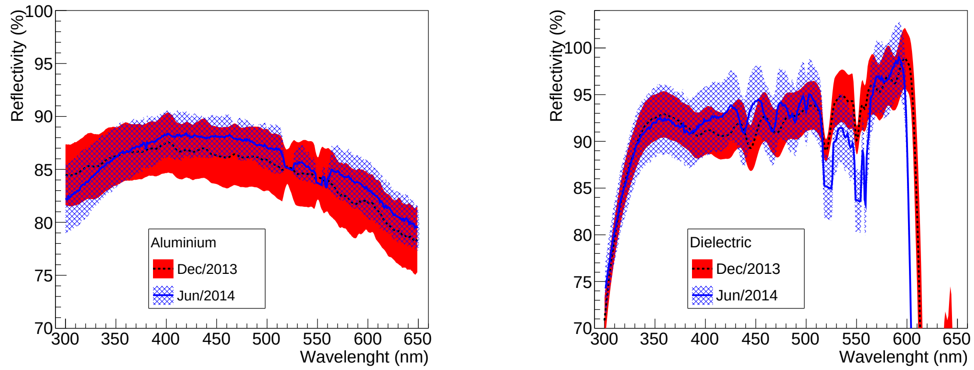

(a) (b)

Figure 10: Reflectivity as a function of wavelength for (a) aluminium and (b) dielectric mirrors. Data was measured in December/2013 (black dashed line - red contour) and June/2014 (full blue line - blue contour). The hatched areas represent the dispersion of the measurement done in 12 (aluminium) and 10 (dielectric) points along the mirror (see figure 6).

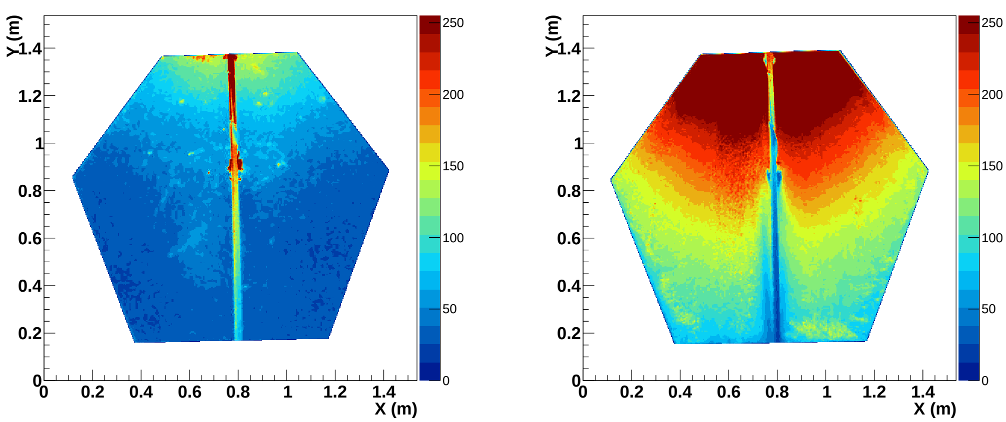

(a) (b)

Figure 11: Color coded map showing the pixel intensity of the pictures taken from (a) a not condensed and (b) a condensed mirror. The vertical feature seen in the middle of the image is a support bar which is removed from further analysis.

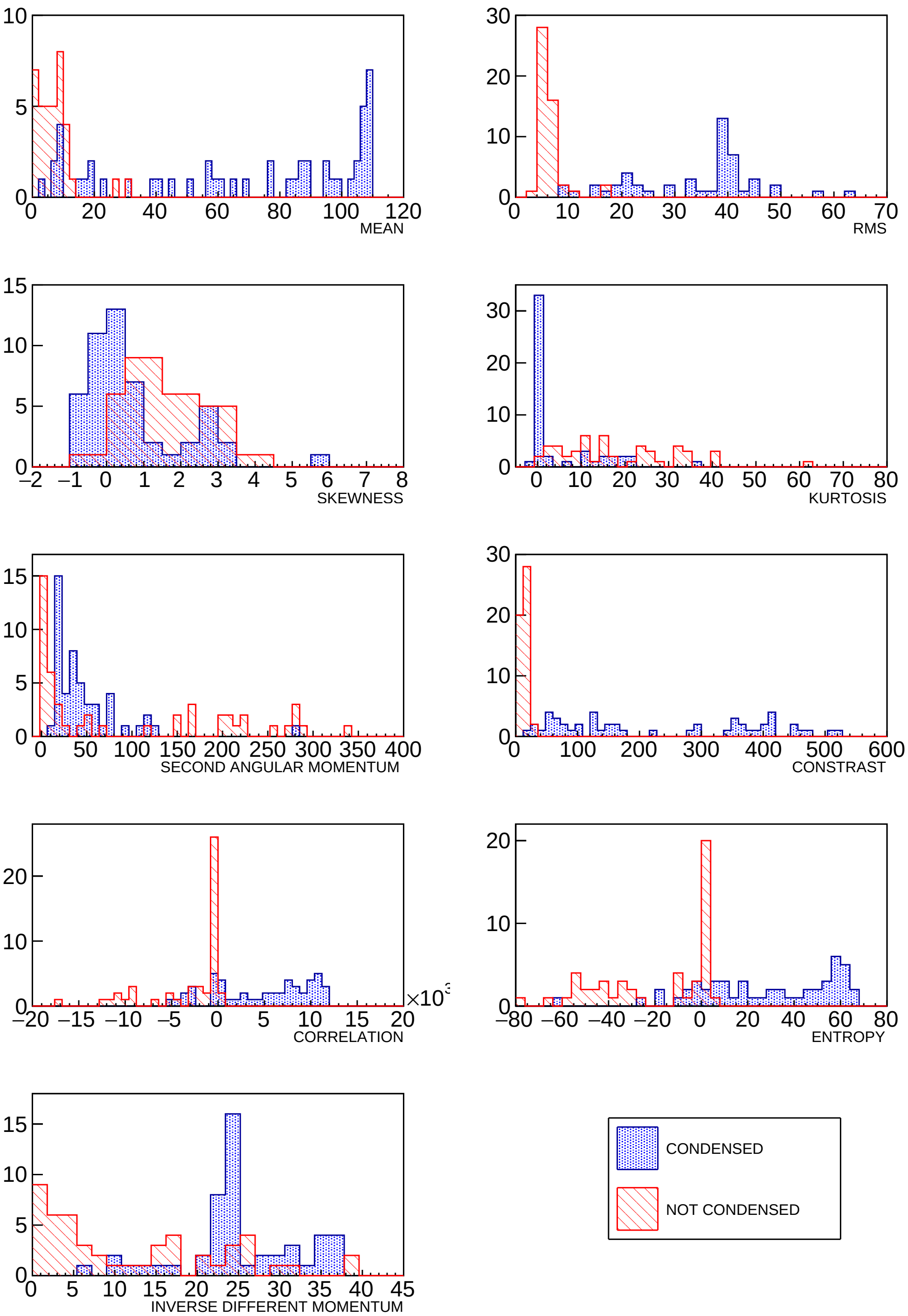

Figure 12: Distribution of the parameters used to discriminate condensed mirrors. See section 3 for details.

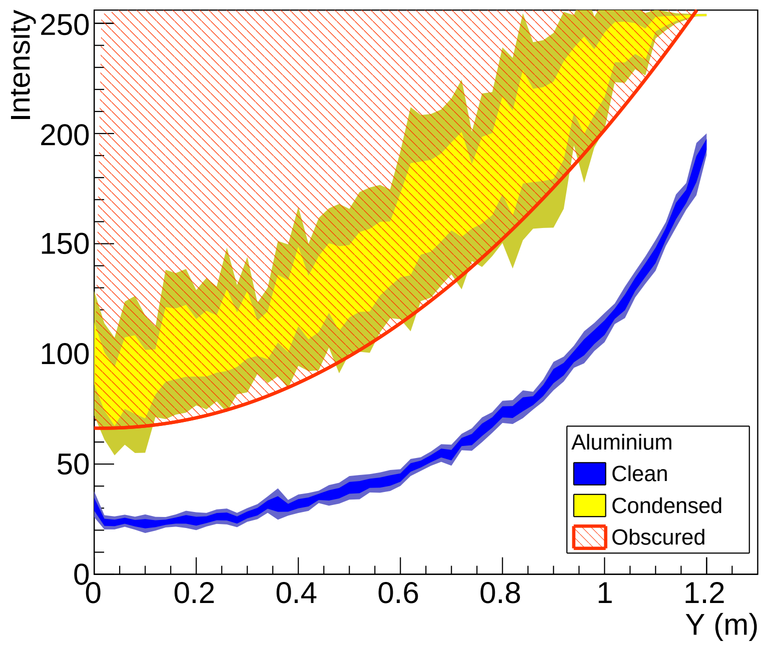

Figure 13: Intensity of light in the picture of the aluminium mirror as a function of height. The blue areas show the one and two sigma region for clean pixels. The yellow areas show the one and two sigma region for condensed pixels. The orange area show the region for which pixels were considered obscured.

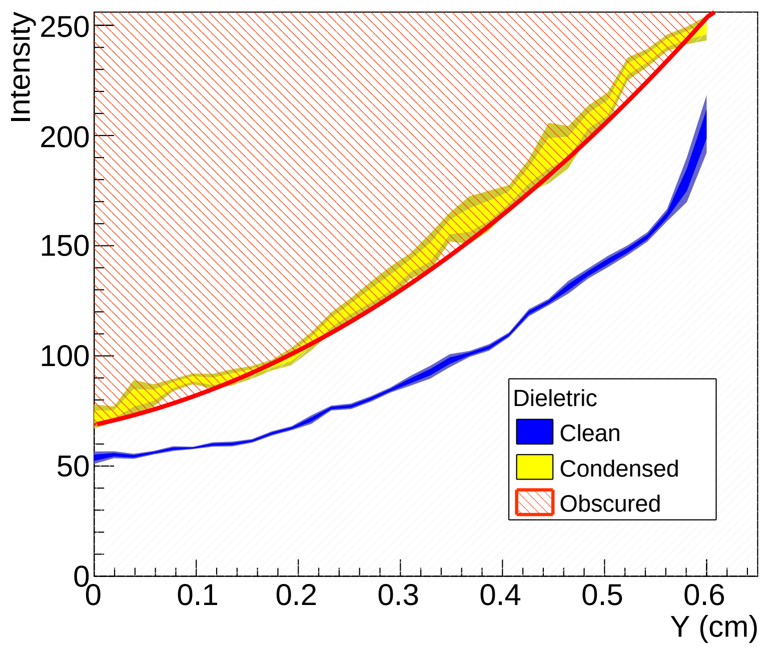

Figure 14: Intensity of light in the picture of the dielectric mirror as a function of height. The blue areas show the one and two sigma region for clean pixels. The yellow areas show the one and two sigma region for condensed pixels. The orange area show the region for which pixels were considered obscured.

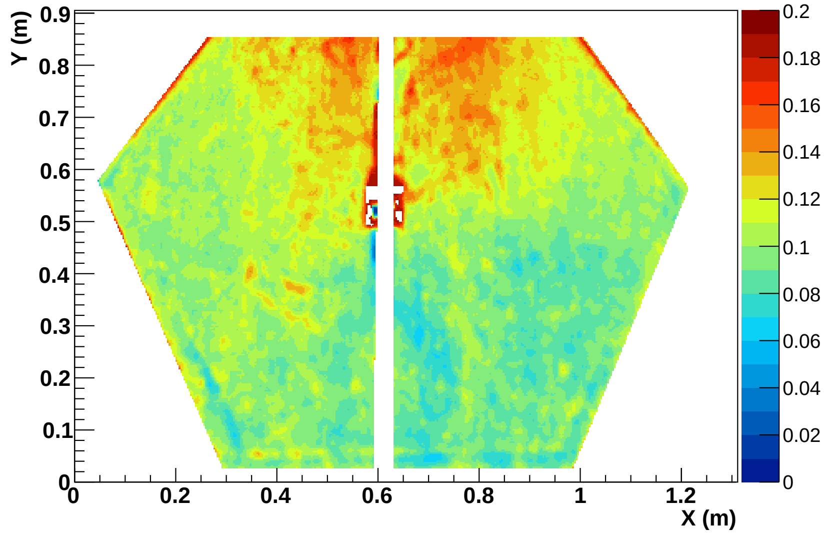

Figure 15: Color coded map representing the percentage of time for which the area of the aluminium mirror was condensed.

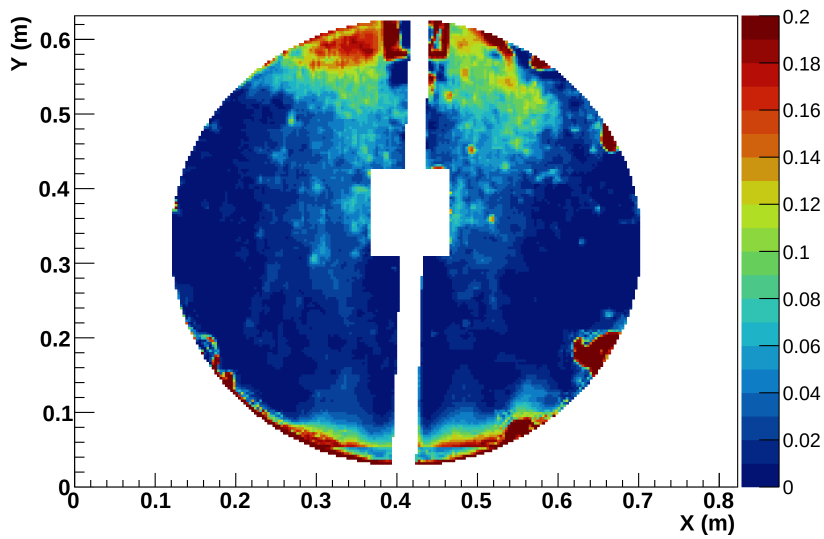

Figure 16: Color coded map representing the percentage of time for which the area of the dielectric mirror was condensed.

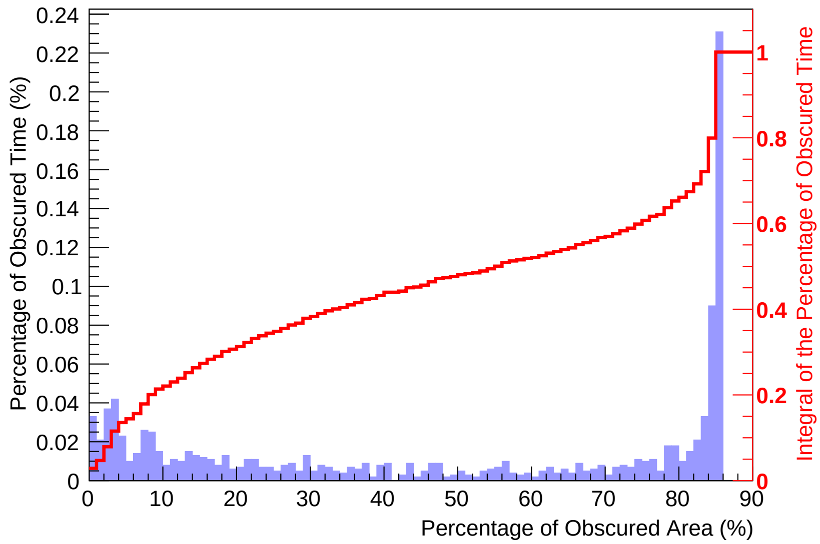

Figure 17: Time versus percentage of condensed area versus integral of time for the aluminium mirror.

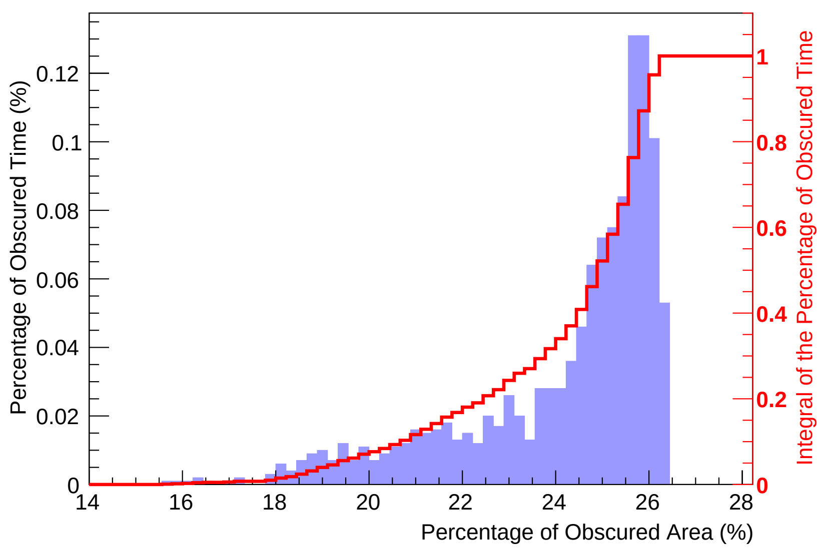

Figure 18: Time versus percentage of condensed area versus integral of time for the dielectric mirror.